Increased crevassing across accelerating Greenland Ice Sheet margins

Thomas R. Chudley
Department of Geography, Durham University, Durham, UK
https://orcid.org/0000-0001-8547-1132

Ian M. Howat
Byrd Polar and Climate Research Center, Ohio State University, Columbus, OH, USA
School of Earth Sciences, Ohio State University, Columbus, OH, USA
https://orcid.org/0000-0002-8072-6260

Michalea D. King
Polar Science Center, University of Washington, Seattle, WA, USA
https://orcid.org/0000-0002-8138-4362

Emma J. MacKie
University of Florida
https://orcid.org/0000-0002-6303-5249

Correspondence: Tom Chudley (thomas.r.chudley@durham.ac.uk)

Increased crevassing across accelerating Greenland Ice Sheet margins

Thomas R. Chudley[1,2], Ian M. Howat[2,3], Michalea D. King[4], Emma J. MacKie[5]

[1] Department of Geography, Durham University, Durham, UK
[2] Byrd Polar and Climate Research Center, Ohio State University, OH, USA
[3] School of Earth Sciences, Ohio State University, OH, USA
[4] Polar Science Center, University of Washington, WA, USA
[5] Department of Geological Sciences, University of Florida, FL, USA

Correspondence: Tom Chudley (thomas.r.chudley@durham.ac.uk)

Abstract

The extent of surface crevassing on the Greenland Ice Sheet is a large source of uncertainty in processes controlling mass loss, including iceberg calving, ice rheology, and water routing. However, no work to date has comprehensively mapped the location of surface crevasses or examined their evolution through time. Here, we use high-resolution digital elevation models to infer the 3-dimensional evolution of crevasse fields across the Greenland Ice Sheet between 2016 and 2021. Whilst the change in the total volume of crevasses was within error (+4.3 ± 5.9%), large and significant increases occurred at accelerating marine-terminating sectors of the ice sheet (up to +25.3 ± 10.1%). These increases were offset only by a reduction in crevasse volume in the central west sector (-14.2 ± 3.2%), particularly at Sermeq Kujalleq (Jakobshavn Isbræ), which underwent a temporary slowdown over the study period. Changes in crevasse volume correlate strongly with antecedent discharge changes, indicating that Greenland's acceleration is affecting significant increases in crevassing on a timescale of less than five years. This rapid response provides a mechanism for mass-loss-promoting feedbacks on sub-decadal timescales, including increased calving, faster flow, and accelerated water transfer to the bed.

Main

Surface crevasses are the direct result of spatial and temporal ice flow variability and, thus, are ubiquitous across the complex and fast-flowing margins of the Greenland Ice Sheet (GrIS). Crevasse formation and propagation exerts a first-order control on glaciological processes as varied as iceberg calving, ice rheology, and glacial hydrology. Fractures can act as pre-existing weaknesses that can promote calving and instability at glacier fronts (Berg & Bassis, 2022; Kneib-Walter et al., 2023), whilst accumulated damage can soften the large-scale rheology of ice (Borstad et al., 2017; Sun et al., 2017; Lhermitte et al., 2020). As a key hydrological pathway (Chudley et al., 2021; Colgan et al., 2011; McGrath et al., 2011), crevasses transfer up to half of

Greenland's seasonal surface runoff to the bed (Koziol et al., 2017). This transport can alter ice rheology by increasing ice temperature (Lüthi et al., 2015; Phillips et al., 2010; Poinar et al., 2017), modify the pressure of the subglacial hydrological system (Cavanagh et al., 2017; Colgan et al., 2011; Lampkin et al., 2013; McGrath et al., 2011), and promote basal melt (Young et al., 2022). By modulating the rate of meltwater transport to the ocean, further influence is exerted on terminus melt, fjord circulation, and fjord biogeochemistry (Bunce et al., 2021; Cowton et al., 2015; Kanna et al., 2022; Slater & Straneo, 2022). These crevasse-dependent processes hold the potential to induce significant feedbacks between ice flow acceleration and mass loss as crevasse field extent increases under larger surface tensile stresses (Colgan et al., 2011, 2015), making them a key source of uncertainty in projections of future Greenland Ice Sheet behaviour.

Given the potential for mass-loss-accelerating feedbacks, understanding how the extent and depth of crevasse fields are changing across Greenland is of key importance. It is expected that increases in crevasse extent have been common across the ice sheet due to a (i) an increase in tensile stresses resulting from both a steepening of the ablation area and outlet glacier acceleration (Colgan et al., 2015), and (ii) an increase in the availability of meltwater available for hydrofracture (Lampkin et al., 2013). However, only one multitemporal study exists, which indicated that crevasse extent increased across a region of West Greenland between 1985 and 2009 (Colgan et al., 2011). These observations are limited to decadal timescales, but observations of surging glaciers have shown that crevasse fields can propagate on much faster timescales (months - years) in response to rapid dynamic change (Herzfeld & Mayer, 1997; Jennings & Hambrey, 2021; Trantow & Herzfeld, 2018). Recent accelerations of outlet glaciers around the GrIS have been of the same order of magnitude as transitions from passive to active surge modes (Bevan et al., 2019; Chudley et al., 2023; Williams et al., 2021), raising the possibility that recent outlet glacier accelerations could initiate significant damage accumulation and subsequent feedbacks over sub-decadal timescales. However, no study has yet monitored short-term change in crevassing in Greenland, nor conducted a comprehensive quantification of crevassing across the full ice sheet.

Recognition of the potential importance of crevassing to mass loss has motivated improved Earth observation and modelling capabilities. Studies have shown that simple parameterisations and fracture criterion used in modelling studies are not a good predictor of crevasse distribution (Chudley et al., 2021; Enderlin & Bartholomaus, 2020; Jennings & Hambrey, 2021) due to mixed-mode fracture formation (Hubbard et al., 2021; van der Veen, 1999), variable ice rheology (Campbell et al., 2013), and the advection of crevasses from zones of active opening (Mottram & Benn, 2009). Therefore, improved observations are important in being able to develop and validate models of fracture formation and propagation (Albrecht & Levermann, 2012; Duddu et al., 2013) and parameterise their behaviour in large-scale models of ice sheet dynamics and hydrology (Clason et al., 2015; Koziol et al., 2017). Observation methods from optical imagery have progressed from manual delineation (Colgan et al., 2011) to computer vision (Gong et al., 2018; Izeboud & Lhermitte, 2023; Van Wyk de Vries et al., 2023) and machine learning (Lai et al., 2020)

approaches, but these have the limitation of assessing only crevasse presence (i.e. 2-D mapping) without critical information about crevasse depth. Attempts to extract crevasse geometry, including depth, have thus far been limited to profiles (Enderlin & Bartholomaus, 2020). However, the recent public availability of comprehensive, multitemporal, and high-resolution digital elevation models (DEMs) of the polar regions from commercial satellite sources (Howat et al., 2022; Porter, Howat, Noh, et al., 2022) provide an unprecedented opportunity to assess 3-D crevasse geometry and evolution at high spatial and temporal resolution. Here we use these data to present the first, time-evolving, three-dimensional record of crevassing over the entire Greenland Ice Sheet during a period of significant changes in ice flow and mass balance. We use this map to quantify the rate and extent of regional trends in crevassing and provide the first ice-sheet-wide observational evidence of the relationship between crevassing and ice dynamic change.

Results

Multitemporal Greenland-wide crevasse inventories

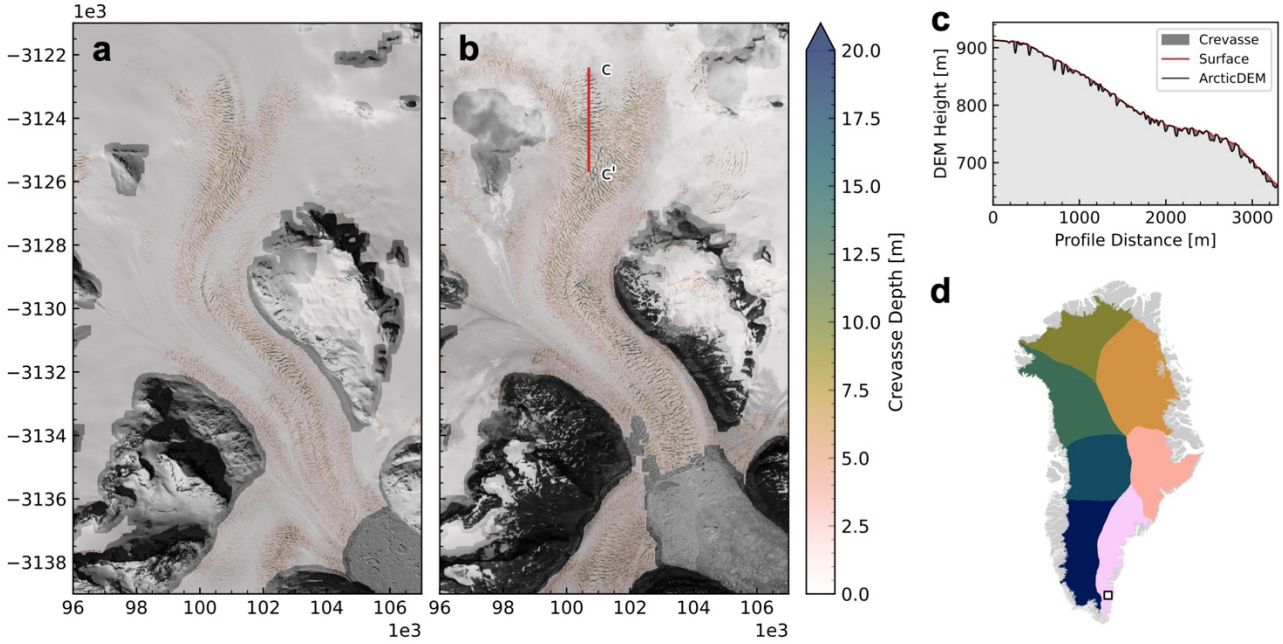

Figure 1: Examples of crevasse field extraction and evolution from ArcticDEM strips. *(a) Crevasse depths obtained from an ArcticDEM strip of a glacier at the head of Anorituup Kangerlua fjord on 2016-04-13, overlaid onto a contemporaneous Worldview-1 image. Coordinates are in NSIDC Polar Stereographic North (b) Same as in (a), but for 2021-07-15 after a period of sustained acceleration and retreat, overlaid onto a contemporaneous Worldview-3 image. Transect c-c' identifies profile presented in panel c. (c) 2D profile along transect c-c', with the raw DEM elevation in black and inferred crevasse depth in red. (d) location of Anorituup Kangerlua fjord within Greenland (white box). Coloured sectors of the ice sheet refer sectors from (Mouginot & Rignot, 2019) sectors, and colours retain continuity of meaning in Fig. 2, 3, and Extended Data Figures.*

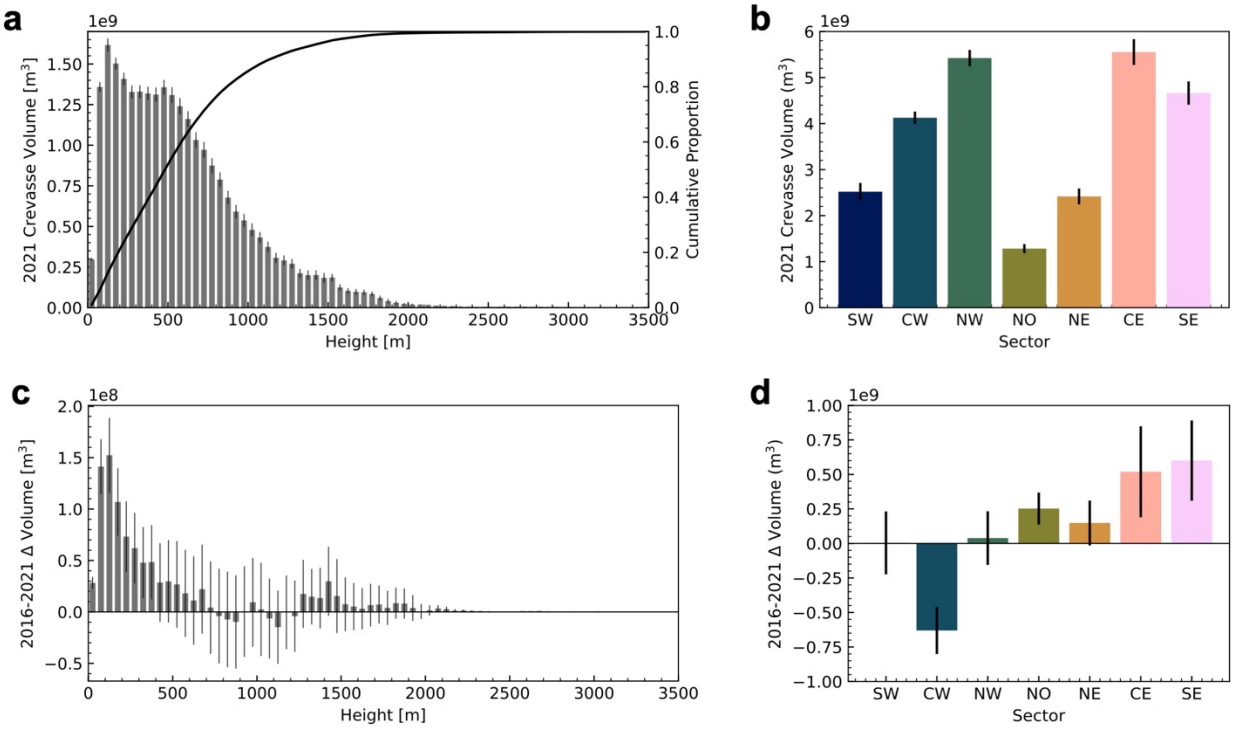

Figure 2: Crevasse volume and changes across the ice sheet. *(a) Histogram of 2021 crevasse volume with surface elevation across the ice sheet. (b) Bar chart of 2021 crevasse volume per sector. (c) Histogram of 2016-2021 crevasse volume change with surface elevation across the ice sheet. (d) Bar chart of 2016-2021 crevasse volume change per sector. Error bars represent 2σ uncertainties (see methods).*

We extracted crevasses from 2 m resolution ArcticDEM strips (Porter, Howat, Noh, et al., 2022) across the GrIS in two years (2016 and 2021). Our method extracts Boolean crevasse presence using a black-top-hat filtering approach (Kodde et al., 2007), before estimating depths as the difference between the raw DEM surface and a 'crevasse-filled' surface approximated via inverse distance weighted interpolation (Fig. 1; Methods). We integrated pixel-based crevasse depth to estimate the air-filled crevasse volume, providing the first estimates of crevasse inventory and change at an ice sheet, sector, and basin scale.

In 2021, we mapped an estimated $25.98 \times 10^9 \pm 1.30 \times 10^9$ m^3 of crevasse volume across ~89% of the melt zone (see Methods) of the GrIS. Crevasse distribution overwhelmingly dominated low elevations near the ice margin (Fig. 2a), with 68% of crevasse volume concentrated below 700 m above mean sea level (AMSL), and 95% below 1420 m AMSL. However, crevasses were less present at the lowest elevations, below 100 m AMSL (Fig. 2a), mostly due to the height of marine-terminating ice cliffs (Parizek et al., 2019). Significant sectoral variation was observed (Fig. 2b), with high volumes of crevasses in the CE, NW, SE, and CW sectors (sectors typified by large, fast-flowing, marine outlets), and lower volumes in the land-terminating SW and less-dynamic NO and NE sectors. The crevasse elevation distribution was also highly variable between sectors (Extended Data Fig. 1). Sector NW exhibited a sharp elevation gradient in crevasse volumes, rapidly decreasing above 1000 m AMSL, whilst the similarly marine-terminating SE and CE sectors

had longer-tailed distributions up to 2000 m AMSL. We suggest that this reflects the typical long trunks of SE/CE sectors, which extended diffusive acceleration from the ice front along their length (and thus elevation), whilst NW glaciers are closely linked to the surrounding ice sheet with strongly convergent flow until close to the glacier margins (Howat et al., 2007; Moon et al., 2012). Sector NO (and, partially, NE) was characterised by an extreme low-elevation bias, with a major peak in the 50-150 m bins and little crevassing above. This likely reflects the predominance of crevassing on floating ice tongues, which are concentrated in these sectors (Reeh, 2017). Finally, the unique distribution of sector CW, with the bulk of crevassing between the 200-800 m AMSL elevation bands, likely reflects the dominance of large marine-terminating outlets with short trunks and high calving fronts such as Sermeq Kujalleq (Jakobshavn Isbræ) (hereafter SKJI).

Between 2016 and 2021, the change in crevasse volume across the Greenland Ice Sheet was statistically insignificant at a 2σ level, with a total change in crevasse volume of $+9.32 \times 10^8 \pm 13.01 \times 10^8$ m^3 (+4.3 ± 5.9%). However, the total masks spatially heterogeneous behaviour by elevation and sector. Beneath 400 m AMSL, crevasse volume increased significantly across all elevations, peaking at 100-150 m AMSL (Fig. 2c). Beneath ~100 m AMSL, increased crevassing was offset by a loss of surface area as marine-terminating glaciers retreated. As with total volume, changes were highly heterogeneous at a sectoral level (Fig. 2d), varying between +25.3 ± 10.1% in the NO to -14.2 ± -3.2% in the CW. No significant changes were observed in the NW or NE, nor the land-terminating SW, whilst significant increases in the NO, CE, and SE were offset by a large reduction in the volume of crevasses in the CW sector (fig. b). Again, sectors displayed distinct elevation distributions (Extended Data Fig. 2). In the NO and NE, increases were limited to ice tongues at the lowest elevations (<~400 m AMSL), whilst increases in the CE and SE were distributed more evenly across the lowest ~1000 m AMSL due to diffusive thinning along the trunk.

Relationship to dynamics

Conventional wisdom holds that changes in crevasse morphology and extent likely reflect changes in ice dynamics: specifically, the surface stress regime (Colgan et al., 2016; van der Veen, 1998; Vaughan, 1993). We used records of total ice flux through outlet glacier termini, termed discharge (King et al., 2020; Mankoff et al., 2020) as a proxy for the bulk dynamic change of ice sectors and basins, assuming that the time-evolving discharge, ice velocity, and the magnitude/extent of extensional stress are broadly correlated at a basin and sectoral scale. Further, as discharge is a function of both ice velocity and outlet size, comparing bulk crevasse volume to bulk discharge implicitly controlled for available ice surface area, unlike direct measurements of ice flow velocity or strain rates. This proposed relationship between discharge and crevasse volume holds at a sectoral scale in our dataset (Fig. 3a; $p = 0.04$). Sectors with high proportions of slow-flowing, land-terminating margins (SW), or less dynamic, well-buttressed outlet glaciers (NO/NE) exhibited low crevasse volumes compared to sectors with high numbers of fast-flowing marine-terminating outlets (SE/CE/NW/CW).

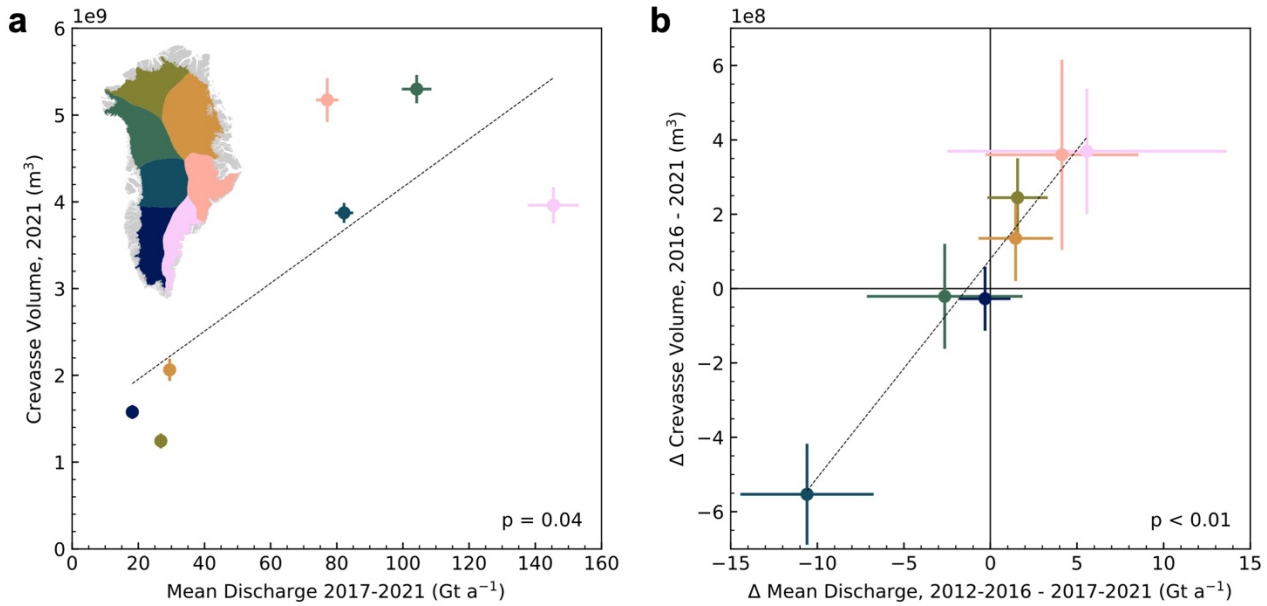

Figure 3: Sectoral-scale discharge comparison. *(a) Scatter plot showing sectoral-scale relationships between 2017-2021 mean annual discharge and 2021 crevasse volume. Error bars represent 2σ uncertainties. (b) Scatter plot showing sectoral-scale relationship between change in mean annual discharge between the 2011-2016 and 2017-2021 periods and change in crevasse volume between 2016-2021. Error bars represent 2σ uncertainties. Note that only drainage basins with significant (>60%) crevasse observations and valid discharge records are included in the sectoral sum totals.*

We found a striking, sector-scale relationship (fig. 3b; $p < 0.01$) between the change in crevasse volumes between 2016-2021 and the change in the antecedent five-year mean discharge (between 2012-2016 and 2017-2021; see Methods), consistent with the hypothesis that changes in crevasse volume and extent are forced by changes in the dynamic regime of glaciers. Reductions in discharge from the CW sector in the second half of the 2010s are well documented (King et al., 2020; Mankoff et al., 2020), largely driven by SKJI, which accounts for ~30% of the regional discharge (King et al., 2020) and has exhibited significant slowdown since 2014 following a reduction in ocean forcing (Joughin et al., 2020; Khazendar et al., 2019). Meanwhile, increased crevassing across the CE and SE sectors were consistent with accelerating ice velocities and discharge observed at both glacier and sectoral levels, linked to warming air and ocean temperatures (Bevan et al., 2019; Black & Joughin, 2022; Chudley et al., 2023; Joughin et al., 2018; Liu et al., 2022).

We further assessed crevasse volume and changes at a basin level (Fig. 4a-b). This analysis confirmed a significant positive relationship ($p < 0.01$) between discharge and crevasse volume (Fig. 4c). However, more nuance is revealed in the relationship between change in discharge and change in crevassing (Fig. 4d). Although there remained a significant relationship between an increase in discharge and an increase in crevassing ($p < 0.01$ where Δ discharge > 0), there appeared to be a weaker relationship between crevassing and a decrease in discharge: in fact, the only glacier to display a significant reduction in both discharge and crevassing was SKJI. After

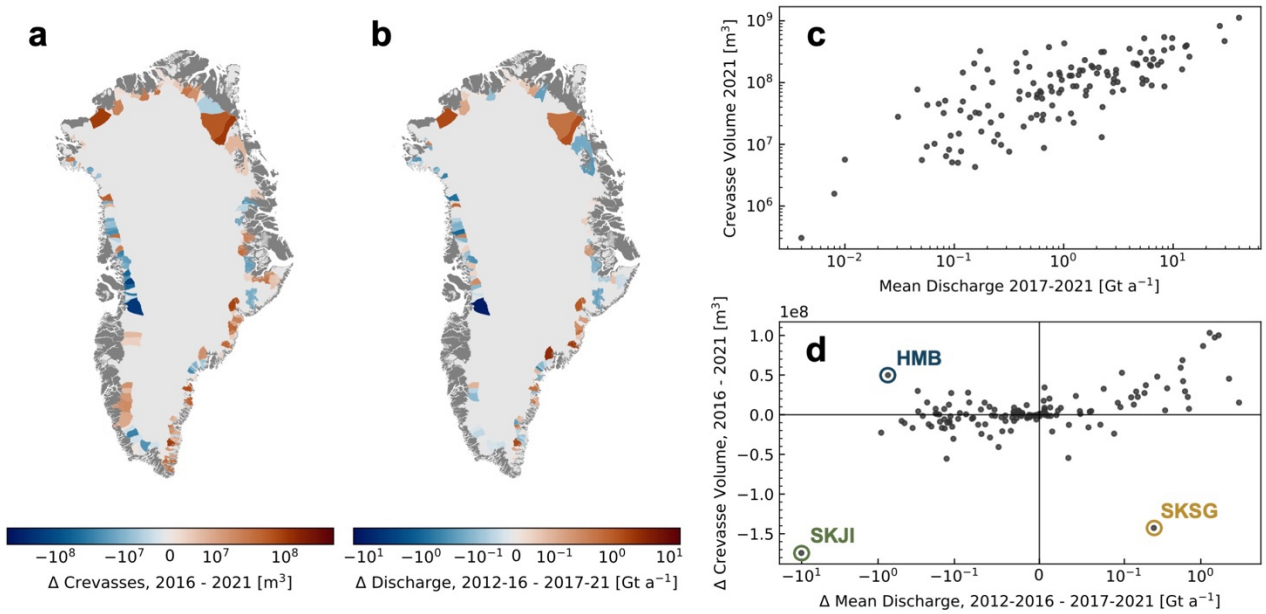

Figure 4: Basin-scale discharge comparison. *(a) Map showing change in crevasse volume between 2016-2021 at a basin scale, where coverage is significant (>60% of total basin area). (b) Map showing change in mean annual discharge between the 2011-2016 and 2017-2021 periods at a basin scale. (c) Scatter plot showing basin-scale relationship between 2017-2021 mean annual discharge and 2021 crevasse volume. (d) Scatter plot showing basin-scale relationship between change in mean annual discharge between the 2011-2016 and 2017-2021 periods and change in crevasse volume between 2016-2021. Outliers Harald Moltke Bræ (HMB), Sermeq Kujalleq (Jakobshavn Isbræ; SKJI), and Sermeq Kujalleq (Store Glacier; SKSG) are labelled. Only basins of a total area > 100 km² are shown.*

excluding SKJI, the relationship was not significant (p = 0.44 where Δ discharge < 0). We suggest this could relate to differing timescales required to open and close crevasse fields, consistent with previous work that has concluded that crevasse formation outpaces crevasses closure (Colgan et al., 2016; Hambrey & Müller, 1978; Harper et al., 1998). Opening of crevasse fields likely occurs rapidly (less than the five-year timescale explored in this study), forced by the higher tensile surface stresses occurring alongside ice acceleration. However, an equivalent reduction in velocity at outlet glaciers does not necessitate a compressive stress regime that would actively close crevasses. Instead, the closure of crevasse fields requires the generational replacement of individual crevasses within a field by smaller crevasses created under lower-tensile-stress conditions. This means that any reduction in crevasse field volume is rate-limited by the surface advection rate. The reduction in crevasse volume shown here at SKJI (labelled in Fig. 4d) may be an instructive exception, demonstrating how the fast-flowing regime enabled crevasse closure to propagate within the five-year timescales explored in this study. An alternative explanation is that the rapid collapse in velocities at SKJI after 2016 (Khazendar et al., 2019) induced a sufficiently large regions of compression (Howat et al., 2007) to actively close crevasses on a short timescale.

Further individual basin-level anomalies also provide interesting insights into crevasse behaviours. For instance, Harald Moltke Bræ (HMB in Fig. 4d) showed distinct reduction in discharge yet an increase in crevassing. This was likely an aliasing effect related to the surge occurring 2013-2019

(Müller et al., 2021), which resulted in an increase in (relict) crevasses in 2021 relative to 2016 even as the discharge reduced between 2012-16 and 2017-21. Sermeq Kujalleq (Store Glacier) (SKSG hereafter and in Fig. 4d) exhibits the opposite anomaly, undergoing significant decreases in crevasse volume despite an increase in discharge. We hypothesise that one potential cause may relate to rapid summer deceleration events that occurred in 2018 and 2019 (Supplementary Fig. 2). SKSG consistently displays 'type-3' seasonal behaviour, undergoing short-term decreases in flow velocity during the ablation season, likely associated with instabilities in basal hydrology and sliding (Moon et al., 2014; Vijay et al., 2021). However, the deceleration events in these two summers were particularly extreme relative to surrounding years, with velocity collapsing by as much as 50% in 2019 (Supplementary Fig. 2), and the resulting perturbation to the glacier strain field may have contributed to a reduction crevasse volume. If these seasonal deceleration events were contributory factors, the magnitude and variability of type-3 seasonality may have an outsized impact on crevasse evolution.

Discussion

We provide the first, Greenland-wide observations of crevasse volume and distribution, revealing significant changes in crevasse fields (sectoral-scale variation from -14.2% to +25.3%) on a timescale an order-of-magnitude faster than previously identified (Colgan et al., 2011). Although total change (+4.3 ± 5.9%) is not significant at a 2σ level, the increase in crevassing in most sectors (Fig. 2d) is offset by only a few glaciers in the CW sector – in particular SKJI, which is known to have undergone a significant slowdown between 2016-2019 (Khazendar *et al.* 2019). Recent data indicate that SKJI is once again exhibiting acceleration and associated dynamic thinning (Khan et al., 2022), suggesting that crevassing may once again be expected to increase here in the coming years alongside other marine-terminating sectors.

The ability to observe the evolution of ice surface features, such as crevasses, in three dimensions and at high spatial resolution over large areas provides a major advance over two-dimensional mapping from imagery alone (Izeboud & Lhermitte, 2023; Van Wyk de Vries et al., 2023). This progress has allowed us to show that the most significant changes in crevasse geometries between 2016-2021 occurred not at the inland margins of crevasse fields, as might be expected if crevasse fields were increasing in extent, but instead occurred at the lowest elevations due to the deepening of pre-existing crevasse fields in trunks and outlets. This aligns with the understanding that crevasse distribution is strongly controlled by the influence of bedrock topography on surface stress fields (Colgan et al., 2016), and suggests that changes in spatial patterns are less important that an increase in pre-existing damage, barring regions where dramatic increases and changes in velocity patterns occur.

If, as shown, externally forced (ocean- or atmosphere-driven) dynamic accelerations can lead to significant increases in outlet glacier crevasse intensity on sub-decadal timescales, there is the potential for a number of positive feedbacks to ice loss to through established mechanisms

(Colgan et al., 2016). The increased accumulation of damage over annual timescales can act to enhance creep and thus flow velocity (Benn & Åström, 2018; Krug et al., 2014), particularly via the structural weakening of shear margins. Crevasses act as pathways for water to reach the bed (Clason et al., 2015; Colgan et al., 2011; Koziol et al., 2017), which can act to warm the ice column and induce further rheological changes (Colgan et al., 2015; Lüthi et al., 2015), modify basal friction (Colgan et al., 2011), and – upon reaching the ocean – amplify submarine melting at the terminus (Slater & Straneo, 2022). Finally, crevasses advected to the calving front play a role in accelerating glacier calving (Berg & Bassis, 2022; Krug et al., 2014), even those forming tens of kilometres inland (Hubbard et al., 2021). The ice-sheet-wide methods, datasets, and behaviours presented here provide a starting point to properly calibrate and validate damage representation in large-scale dynamic models, allowing the community to accommodate the effects of ice damage and crevassing into predictions of future ice sheet behaviour.

Methods

Crevasse Detection

Crevasse depth detection from ArcticDEM strips

We mapped crevasses using 2-m resolution ArcticDEM v4.1 strips (Porter, Howat, Noh, et al., 2022) provided by the Polar Geospatial Center (PGC). The method, which we make public as a Python package and associated Jupyter Notebooks (https://github.com/trchudley/crevdem), will also work on other 2 m strips provided by the PGC as part of the REMA (Howat et al., 2022) or EarthDEM (Porter, Howat, Husby, et al., 2022) projects, although we cannot guarantee the optimal length scale we determine here is representative of other sectors of the Cryosphere. We first preprocessed the strips by filtering them only to good-quality ice surfaces. This was done by filtering strips to 'good' data as indicated by the PGC-provided bitmasks; filtering out bedrock using the Greenland Ice Mapping Project (GrIMP) Ice and Ocean classification mask (Howat et al., 2014); and geoid-correcting the heights to mean sea level using the EIGEN-6C4 geoid model (Förste et al., 2014) provided within BedMachine v4 (Morlighem et al., 2017). Finally, when over 1 km^2 of strip area is < 10 m above mean sea level (AMSL), we applied a routine to filter out 'marine surfaces' (ocean, sea ice, and low-lying ice mélange) following a previously published iceberg detection routine (Shiggins et al., 2023). In this approach, we constructed a histogram of elevation in 0.25 m bins between -15 and +15 m AMSL, and identified contemporaneous sea level as the modal bin. We assigned all regions beneath 10 m of our determined contemporaneous sea level as marine surfaces, leaving only terrestrial ice and floating ice tongues.

After pre-processing, we determined the observed open-air crevasse depth, which we define here as the difference between the raw DEM height and a nominal 'filled crevasse' surface. We first detrended the DEM using a large Gaussian filter (standard deviation 200 m), before applying a black top hat (BTH) filter to the detrended surface to determine the negative deviation from the

local maxima (Kodde et al., 2007). Gaussian and BTH filters were both applied using OpenCV implementations (Bradski, 2000). The diameter of the BTH kernel was set to be 60 m, following spatial variogram analysis of crevassed surfaces around Greenland (see section 'Determining the optimal crevasse length scale'). We identify pixels as 'crevassed' where the BTH-filtered value is > 1 m. To generate a nominal 'crevasse-filled' surface, we removed the crevassed pixels and filled the surfaces using an inverse-distance weighting algorithm as implemented in GDAL (Rouault et al., 2023), followed by two 3×3 averaging filter smoothing operations to dampen artefacts. Crevasse depth was determined as the difference between the interpolated 'surface' and the crevasse bottom in the raw DEM.

Determining the optimal crevasse length scale

A key quantitative variable that informed our kernel-based detection algorithm was the length scale of the crevasses. We assessed this by modelling the spatial covariance, or variogram, which quantifies the variance of spatial measurements as a function of their separation distance (Matheron, 1963). The variogram was used to determine the range, or separation distance at which measurements are spatially uncorrelated. The range parameter has previously been used to determine the optimal kernel size for BTH filtering of DEMs (Kodde et al., 2007). To find a representative range parameter, we estimated the ranges at four different glaciers covering a range of sectors and dynamic contexts: Sermeq Kujalleq (Jakobshavn Isbræ), Sermeq Kujalleq (Store Glacier), KJV Steenstrups Nordre Bræ, and Isunnguata Sermia. We manually identified five 1500 × 1500 m sample zones, which we subjectively ranked on an ordinal scale of 'crevasse intensity' from 0 (no crevasses) to 4 (most crevassed region of glacier). We then constructed spatial variograms of the five sample zones using SciKit-GStat (Mälicke, 2022). We used a detrended 2021 sample DEM (Supplementary Fig. 2-5), randomly sampling 2% of the pixels within the sample zone to increase computational efficiency. To estimate the representative crevasse width, we used the range of the variograms as estimated using a Gaussian variogram model. The mean estimated spatial range of the most crevassed sample regions (crevasse intensity = 4) was 62.4 m; the mean estimated spatial of the top two most crevassed regions (crevasse intensity ≥ 3) was 57.3 m (Supplementary Fig. 2-5). We selected 60 m as a representative range (and thus kernel size) to apply to fast-flowing regions of the Greenland Ice Sheet.

Ice-sheet wide processing and mosaicking

We produced GrIS-wide maps of crevasses in 2016 and 2021, years when ArcticDEM strip coverage was high and particularly conducive to comprehensive assessment.

To eliminate extraneous processing in the ice interior, we generously defined an AOI mask as anywhere melt occurs in the RACMO2.3p2 1 km melt model between 2016 and 2021 (Noël et al., 2019), dilated by 10 km. We took all strips intersecting this region between April and October with a reported RMSE < 2 m and a component image baseline < 60 minutes. In total, we processed 4667 strips in 2016 and 4207 strips in 2021 (Supplementary Table 1), with a subsequent coverage of our AOI of 75% and 86% respectively (Supplementary Fig. 6). We note that coverage is biased

towards outlet glaciers and no-data regions are commonly high-elevation, low-velocity sectors in the accumulation zone. This benefits our assessment as no-data regions are largely regions without crevassing present.

Due to the advection of individual crevasses, 2 m resolution crevasse depth maps cannot be directly compared. Instead, we enabled comparison between 2016 and 2021 by summing crevasse depth maps into 200 m resolution crevasse volume maps, which we refer to as the 'exposed crevasse air volume'. To obtain a single annual mosaic, we found the median value of all overlapping strips where multiple exist. We present crevasse volume change aggregated into established sectors and basins (Mouginot & Rignot, 2019).

Uncertainty

We assigned an uncertainty to our aggregate crevasse volume measurements by assessing variation in contemporaneous strip measurements. To do this, we assessed variance within the Nioghalvfjerdsfjorden (79˚N) discharge basin in 2021, which we selected due to its high overlapping strip records (up to 21 overlapping strips) and large variation in surface types. Across all valid pixels within the 79˚N area of interest, the mean standard deviation of strip volumes within 200 m grid cells was 407 m^3 (10,175 m^3 km^{-2}). We present 2σ error bars within the figures presented in this paper.

Limitations

The limitations of our dataset are derived from the resolution and optical source data of the raw ArcticDEM strips.

First, the 2 m resolution of the source strips places a fundamental lower bound on the minimum identifiable crevasse diameter. In practice, comparison with UAV data has shown that a realistic minimum diameter observable with these methods is ~10 m (Chudley et al., 2021). Although this limits applications for smaller inland crevasses, it is more than sufficient for observation of changes at crevasse fields in fast-flowing (>100 m/a) regions, where the crevasse width averages ~60 m (see section 'Determining the optimal crevasse length scale').

Second, the reported crevasse depth values produced by our method are commonly in the range of 10-100 m deep. This does not represent full crevasse depth, as even crevasses with surface expressions of only 10s of centimetres have been shown reach depths of hundreds of metres (Hubbard et al., 2021). However, larger crevasses of the type observed in this study (~10s metres in width) have been observed to be consistently infilled with debris in high-resolution UAV-derived datasets (Chudley et al., 2019), limiting the observed depth in optically-derived DEMs. As such, we refer to the volumetric measurements in this study as the 'exposed crevasse air volume', acknowledging that full-depth measurements are not possible. Full crevasse depths have

extrapolated from simpler 2D profiles in the past (Enderlin & Bartholomaus, 2020), suggesting that a similar method to extrapolate 3D datasets may be possible in the future.

Third, the optical nature of the source data meant that we cannot extract snow-filled crevasses that may be possible to detect using other methods, such as SAR or GPR (Thompson et al., 2020). However, the large diameters of crevasses detected here are highly unlikely to fill with snow (Van Wyk de Vries et al., 2023), especially in a Greenlandic context where most major crevasse fields are located deep into the ablation zone. The month filtering and median filtering we performed during the mosaicking process mean we consider it very unlikely that snowfill can explain any of the large-scale multitemporal change we observe in our study.

Finally, by selecting a relatively shallow BTH threshold of 1 m, we implicitly included features that are not true crevasses (e.g. shallow ditches and river gulleys). We chose to do this as we are interested in volumetric change rather than area change, and these shallow features do not represent significant contributions to aggregate volume measurements. Increasing the BTH threshold to a higher value introduces a much larger volume of false negatives instead of a small volume of false positives. Experimentation showed that increasing the threshold for crevasse identification may aesthetically improve the binary crevasse mask, but resulted in an increased variance in our volumetric uncertainty measurements as legitimate crevasses began to be inconsistently masked from DEM strips.

Discharge

We compared crevasse change to discharge change as a proxy for the bulk dynamic change of ice sectors and basins. Changes in dynamic forcing takes time to propagate through to observed changes in crevasse fields, as crevasses are the product of opening and closing stresses integrated over multiple years. As a result, we compared the average annual discharge for the preceding five years (2012-2016 for the 2016 crevasse dataset and 2017-2021 for the 2021 dataset). A period of 5 years was selected to be in line with published estimates of crevasse lifecycles in studies of valley glaciers (Harper et al., 1998; Meier, 1958) and ensured discharge records do not overlap.

We obtained 2012-2021 monthly ice discharge measurements from flux gate measurements at marine-terminating glaciers from two complimentary datasets (King et al., 2020; Mankoff et al., 2020) (hereafter the ‘King’ and ‘Mankoff’ datasets). Each individual dataset covers specific outlet glaciers, and neither is comprehensive across all Greenland outlets. As the pre-defined drainage basins (Mouginot & Rignot, 2019) frequently contain multiple outlets, any individual drainage basin may be comprehensively covered by flux gates from either the King or Mankoff datasets, both, or neither. As a result, we combined the datasets to cover as many discharge basins as possible. Of the 254 basins in the dataset, we assessed 192 as having discharge records in at least one dataset. Of these, 185 basins were usable. 138 had outlets comprehensively covered by both King

and Mankoff, so we took the average of the two datasets. 29 and 16 basins were comprehensively covered only by King or Mankoff respectively. At two basins, unusually, the two datasets covered mutually exclusive outlets within the basin, and we used the sum of the two datasets to represent full basin discharge.

Data Availability

Source data (necessary to reproduce this study and the figures within (Greenland-wide crevasse volume rasters, and basin-scale aggregations of crevasse volume and discharge) have been deposited in a Figshare repository available at https://doi.org/10.6084/m9.figshare.23937654. ArcticDEM 2 m strips are available at https://doi.org/10.7910/DVN/OHHUKH. The EIGEN-6C4 model is available as part of the BedMachine v4 at https://doi.org/10.5067/VLJ5YXKCNGXO. The GrIMP ice and ocean classification mask is available at https://doi.org/10.5067/B8X58MQBFUPA. Raw Mankoff discharge data is available at https://doi.org/10.22008/promice/data/ice_discharge.

Code Availability

The full workflow to download and extract crevasses from ArcticDEM and REMA imagery is publicly available as a Python package at https://github.com/trchudley/crevdem.

Acknowledgements

This project was supported by grants from the National Aeronautics and Space Administration (NASA; 80NSSC18K1027 and 80NSSC18M0078) and National Science Foundation Office for Polar Programs (NSF-OPP; A007467501) awarded to IMH. TRC was supported by a Leverhulme Early Career Fellowship (ECF-2022-589). MDK was supported by NASA (80NSSC22K1709). ArcticDEM strips are provided by the Polar Geospatial Center under NSF-OPP awards 1043681, 1559691, and 1542736. We are grateful to Chris Stokes for discussions regarding this paper.

Author contributions

TRC: Conceptualisation, methodology, software, formal analysis, investigation, writing – original draft, writing – review & editing, visualisation, funding acquisition.
IMH: Conceptualisation, methodology, writing – review & editing, supervision, project administration, funding acquisition.
MDK: Formal analysis, investigation, writing – review and editing.
EJM: Methodology, formal analysis, writing – review & editing.

Ethics declaration

The authors declare no competing interests.

References

Albrecht, T., & Levermann, A. (2012). Fracture field for large-scale ice dynamics. *Journal of Glaciology*, *58*(207), 165–176. https://doi.org/10.3189/2012JoG11J191

Benn, D. I., & Åström, J. A. (2018). Calving glaciers and ice shelves. *Advances in Physics: X*, *3*(1), 1513819. https://doi.org/10.1080/23746149.2018.1513819

Berg, B., & Bassis, J. (2022). Crevasse advection increases glacier calving. *Journal of Glaciology*, *68*(271), 977–986. https://doi.org/10.1017/jog.2022.10

Bevan, S. L., Luckman, A. J., Benn, D. I., Cowton, T., & Todd, J. (2019). Impact of warming shelf waters on ice mélange and terminus retreat at a large SE Greenland glacier. *The Cryosphere*, *13*(9), 2303–2315. https://doi.org/10.5194/tc-13-2303-2019

Black, T. E., & Joughin, I. (2022). Multi-decadal retreat of marine-terminating outlet glaciers in northwest and central-west Greenland. *The Cryosphere*, *16*(3), 807–824. https://doi.org/10.5194/tc-16-807-2022

Borstad, C., McGrath, D., & Pope, A. (2017). Fracture propagation and stability of ice shelves governed by ice shelf heterogeneity. *Geophysical Research Letters*, *44*(9), 4186–4194. https://doi.org/10.1002/2017GL072648

Bradski, G. (2000). The OpenCV Library. *Dr. Dobb's Journal: Software Tools for the Professional Programmer*, *25*(11), 120–123.

Bunce, C., Nienow, P., Sole, A., Cowton, T., & Davison, B. (2021). Influence of glacier runoff and near-terminus subglacial hydrology on frontal ablation at a large Greenlandic tidewater glacier. *Journal of Glaciology*, *67*(262), 343–352. https://doi.org/10.1017/jog.2020.109

Campbell, S., Roy, S., Kreutz, K., Arcone, S. A., Osterberg, E. C., & Koons, P. (2013). Strain-rate estimates for crevasse formation at an alpine ice divide: Mount Hunter, Alaska. *Annals of Glaciology*, *54*(63), 200–208. https://doi.org/10.3189/2013AoG63A266

Cavanagh, J. P., Lampkin, D. J., & Moon, T. (2017). Seasonal Variability in Regional Ice Flow Due to Meltwater Injection Into the Shear Margins of Jakobshavn Isbræ. *Journal of Geophysical Research: Earth Surface*, *122*(12), 2488–2505. https://doi.org/10.1002/2016JF004187

Chudley, T. R., Christoffersen, P., Doyle, S. H., Abellan, A., & Snooke, N. (2019). High-accuracy UAV photogrammetry of ice sheet dynamics with no ground control. *The Cryosphere*, *13*(3), 955–968. https://doi.org/10.5194/tc-13-955-2019

Chudley, T. R., Christoffersen, P., Doyle, S. H., Dowling, T. P. F., Law, R., Schoonman, C. M., Bougamont, M., & Hubbard, B. (2021). Controls on Water Storage and Drainage in Crevasses on the Greenland Ice Sheet. *Journal of Geophysical Research: Earth Surface*, *126*(9), e2021JF006287. https://doi.org/10.1029/2021JF006287

Chudley, T. R., Howat, I. M., King, M. D., & Negrete, A. (2023). Atlantic water intrusion triggers rapid retreat and regime change at previously stable Greenland glacier. *Nature Communications*, *14*(1), Article 1. https://doi.org/10.1038/s41467-023-37764-7

Clason, C. C., Mair, D. W. F., Nienow, P. W., Bartholomew, I. D., Sole, A., Palmer, S., & Schwanghart, W. (2015). Modelling the transfer of supraglacial meltwater to the bed of Leverett Glacier, Southwest Greenland. *The Cryosphere*, *9*(1), 123–138. https://doi.org/10.5194/tc-9-123-2015

Colgan, W., Rajaram, H., Abdalati, W., McCutchan, C., Mottram, R., Moussavi, M. S., & Grigsby, S. (2016). Glacier crevasses: Observations, models, and mass balance implications. *Reviews of Geophysics*, *54*(1), 119–161. https://doi.org/10.1002/2015RG000504

Colgan, W., Sommers, A., Rajaram, H., Abdalati, W., & Frahm, J. (2015). Considering thermal-viscous collapse of the Greenland ice sheet. *Earth's Future*, *3*(7), 252–267. https://doi.org/10.1002/2015EF000301

Colgan, W., Steffen, K., McLamb, W. S., Abdalati, W., Rajaram, H., Motyka, R., Phillips, T., & Anderson, R. (2011). An increase in crevasse extent, West Greenland: Hydrologic implications. *Geophysical Research Letters*, *38*(18). https://doi.org/10.1029/2011GL048491

Cowton, T., Slater, D., Sole, A., Goldberg, D., & Nienow, P. (2015). Modeling the impact of glacial runoff on fjord circulation and submarine melt rate using a new subgrid-scale parameterization for glacial plumes. *Journal of Geophysical Research: Oceans*, *120*(2), 796–812. https://doi.org/10.1002/2014JC010324

Duddu, R., Bassis, J. N., & Waisman, H. (2013). A numerical investigation of surface crevasse propagation in glaciers using nonlocal continuum damage mechanics. *Geophysical Research Letters*, *40*(12), 3064–3068. https://doi.org/10.1002/grl.50602

Enderlin, E. M., & Bartholomaus, T. C. (2020). Sharp contrasts in observed and modeled crevasse patterns at Greenland's marine terminating glaciers. *The Cryosphere*, *14*(11), 4121–4133. https://doi.org/10.5194/tc-14-4121-2020

Förste, C., Bruinsma, Sean. L., Abrikosov, O., Lemoine, J.-M., Marty, J. C., Flechtner, F., Balmino, G., Barthelmes, F., & Biancale, R. (2014). *EIGEN-6C4 The latest combined global gravity field model including GOCE data up to degree and order 2190 of GFZ Potsdam and GRGS Toulouse* (p. 55102156 Bytes, 3 Files) [Application/octet-stream,application/octet-stream,application/zip]. GFZ Data Services. https://doi.org/10.5880/ICGEM.2015.1

Gong, Y., Zwinger, T., Åström, J., Altena, B., Schellenberger, T., Gladstone, R., & Moore, J. C. (2018). Simulating the roles of crevasse routing of surface water and basal friction on the surge evolution of Basin 3, Austfonna ice cap. *The Cryosphere*, *12*(5), 1563–1577. https://doi.org/10.5194/tc-12-1563-2018

Hambrey, M. J., & Müller, F. (1978). Structures and ice deformation in the white glacier, Axel Heiberg Island, Northwest Territories, Canada. *Journal of Glaciology*, *20*(82), 41–66. https://doi.org/10.3189/S0022143000021213

Harper, J. T., Humphrey, N. F., & Pfeffer, W. T. (1998). Crevasse patterns and the strain-rate tensor: A high-resolution comparison. *Journal of Glaciology*, *44*(146), 68–76. https://doi.org/10.3189/S0022143000002367

Herzfeld, U. C., & Mayer, H. (1997). Surge of Bering Glacier and Bagley Ice Field, Alaska: An update to August 1995 and an interpretation of brittle-deformation patterns. *Journal of Glaciology*, *43*(145), 427–434. https://doi.org/10.3189/S0022143000035012

Howat, I. M., Joughin, I., & Scambos, T. A. (2007). Rapid Changes in Ice Discharge from Greenland Outlet Glaciers. *Science*, *315*(5818), 1559–1561. https://doi.org/10.1126/science.1138478

Howat, I. M., Negrete, A., & Smith, B. E. (2014). The Greenland Ice Mapping Project (GIMP) land classification and surface elevation data sets. *The Cryosphere*, *8*(4), 1509–1518. https://doi.org/10.5194/tc-8-1509-2014

Howat, I. M., Porter, C., Noh, M.-J., Husby, E., Khuvis, S., Danish, E., Tomko, K., Gardiner, J., Negrete, A., Yadav, B., Klassen, J., Kelleher, C., Cloutier, M., Bakker, J., Enos, J., Arnold, G., Bauer, G., & Morin, P. (2022). *The Reference Elevation Model of Antarctica—Strips, Version 4.1* [dataset]. Harvard Dataverse. https://doi.org/10.7910/DVN/X7NDNY

Hubbard, B., Christoffersen, P., Doyle, S. H., Chudley, T. R., Schoonman, C. M., Law, R., & Bougamont, M. (2021). Borehole-Based Characterization of Deep Mixed-Mode Crevasses at a Greenlandic Outlet Glacier. *AGU Advances*, *2*(2), e2020AV000291. https://doi.org/10.1029/2020AV000291

Izeboud, M., & Lhermitte, S. (2023). Damage detection on antarctic ice shelves using the normalised radon transform. *Remote Sensing of Environment*, *284*, 113359. https://doi.org/10.1016/j.rse.2022.113359

Jennings, S. J. A., & Hambrey, M. J. (2021). Structures and Deformation in Glaciers and Ice Sheets. *Reviews of Geophysics*, *59*(3), e2021RG000743. https://doi.org/10.1029/2021RG000743

Joughin, I., Shean, D. E., Smith, B. E., & Floricioiu, D. (2020). A decade of variability on Jakobshavn Isbræ: Ocean temperatures pace speed through influence on mélange rigidity. *The Cryosphere*, *14*(1), 211–227. https://doi.org/10.5194/tc-14-211-2020

Joughin, I., Smith, B. E., & Howat, I. (2018). Greenland Ice Mapping Project: Ice flow velocity variation at sub-monthly to decadal timescales. *The Cryosphere*, *12*(7), 2211–2227. https://doi.org/10.5194/tc-12-2211-2018

Kanna, N., Sugiyama, S., Ando, T., Wang, Y., Sakuragi, Y., Hazumi, T., Matsuno, K., Yamaguchi, A., Nishioka, J., & Yamashita, Y. (2022). Meltwater Discharge From Marine-Terminating Glaciers Drives Biogeochemical Conditions in a Greenlandic Fjord. *Global Biogeochemical Cycles*, *36*(11), e2022GB007411. https://doi.org/10.1029/2022GB007411

Khan, S. A., Bamber, J. L., Rignot, E., Helm, V., Aschwanden, A., Holland, D. M., van den Broeke, M., King, M., Noël, B., Truffer, M., Humbert, A., Colgan, W., Vijay, S., & Kuipers Munneke, P. (2022). Greenland Mass Trends From Airborne and Satellite Altimetry During 2011–2020. *Journal of*

Geophysical Research: Earth Surface, *127*(4), e2021JF006505. https://doi.org/10.1029/2021JF006505

Khazendar, A., Fenty, I. G., Carroll, D., Gardner, A., Lee, C. M., Fukumori, I., Wang, O., Zhang, H., Seroussi, H., Moller, D., Noël, B. P. Y., van den Broeke, M. R., Dinardo, S., & Willis, J. (2019). Interruption of two decades of Jakobshavn Isbrae acceleration and thinning as regional ocean cools. *Nature Geoscience*, *12*(4), Article 4. https://doi.org/10.1038/s41561-019-0329-3

King, M. D., Howat, I. M., Candela, S. G., Noh, M. J., Jeong, S., Noël, B. P. Y., van den Broeke, M. R., Wouters, B., & Negrete, A. (2020). Dynamic ice loss from the Greenland Ice Sheet driven by sustained glacier retreat. *Communications Earth & Environment*, *1*(1), 1–7. https://doi.org/10.1038/s43247-020-0001-2

Kneib-Walter, A., Lüthi, M. P., Funk, M., Jouvet, G., & Vieli, A. (2023). Observational constraints on the sensitivity of two calving glaciers to external forcings. *Journal of Glaciology*, *69*(275), 459–474. https://doi.org/10.1017/jog.2022.74

Kodde, M. P., Pfeifer, N., Gorte, B. G. H., Geist, T., & Höfle, B. (2007). Automatic glacier surface analysis from airborne laser scanning. *International Archives of the Photogrammetry, Remote Sensing and Spatial Information Sciences*, *36*(3), 221–226.

Koziol, C., Arnold, N., Pope, A., & Colgan, W. (2017). Quantifying supraglacial meltwater pathways in the Paakitsoq region, West Greenland. *Journal of Glaciology*, 1–13. https://doi.org/10.1017/jog.2017.5

Krug, J., Weiss, J., Gagliardini, O., & Durand, G. (2014). Combining damage and fracture mechanics to model calving. *The Cryosphere*, *8*(6), 2101–2117. https://doi.org/10.5194/tc-8-2101-2014

Lai, C.-Y., Kingslake, J., Wearing, M. G., Chen, P.-H. C., Gentine, P., Li, H., Spergel, J. J., & van Wessem, J. M. (2020). Vulnerability of Antarctica's ice shelves to meltwater-driven fracture. *Nature*, *584*(7822), Article 7822. https://doi.org/10.1038/s41586-020-2627-8

Lampkin, D. J., Amador, N., Parizek, B. R., Farness, K., & Jezek, K. (2013). Drainage from water-filled crevasses along the margins of Jakobshavn Isbræ: A potential catalyst for catchment expansion. *Journal of Geophysical Research: Earth Surface*, *118*(2), 795–813. https://doi.org/10.1002/jgrf.20039

Lhermitte, S., Sun, S., Shuman, C., Wouters, B., Pattyn, F., Wuite, J., Berthier, E., & Nagler, T. (2020). Damage accelerates ice shelf instability and mass loss in Amundsen Sea Embayment. *Proceedings of the National Academy of Sciences*, *117*(40), 24735–24741. https://doi.org/10.1073/pnas.1912890117

Liu, J., Enderlin, E., Marshall, H.-P., & Khalil, A. (2022). Synchronous retreat of southeast Greenland's peripheral glaciers. *Geophysical Research Letters*, *n/a*(n/a), e2022GL097756. https://doi.org/10.1029/2022GL097756

Lüthi, M. P., Ryser, C., Andrews, L. C., Catania, G. A., Funk, M., & Hawley, R. L. (2015). Heat sources within the Greenland Ice Sheet: Dissipation, temperate paleo-firn and cryo-hydrologic warming. *The Cryosphere*. https://doi.org/10.5194/tc-9-245-2015

Mälicke, M. (2022). SciKit-GStat 1.0: A SciPy-flavored geostatistical variogram estimation toolbox written in Python. *Geoscientific Model Development*, *15*(6), 2505–2532. https://doi.org/10.5194/gmd-15-2505-2022

Mankoff, K. D., Noël, B., Fettweis, X., Ahlstrøm, A. P., Colgan, W., Kondo, K., Langley, K., Sugiyama, S., van As, D., & Fausto, R. S. (2020). Greenland liquid water discharge from 1958 through 2019. *Earth System Science Data*, *12*(4), 2811–2841. https://doi.org/10.5194/essd-12-2811-2020

Matheron, G. (1963). Principles of geostatistics. *Economic Geology*, *58*(8), 1246–1266. https://doi.org/10.2113/gsecongeo.58.8.1246

McGrath, D., Colgan, W., Steffen, K., Lauffenburger, P., & Balog, J. (2011). Assessing the summer water budget of a moulin basin in the Sermeq Avannarleq ablation region, Greenland ice sheet. *Journal of Glaciology*, *57*(205), 954–964. https://doi.org/10.3189/002214311798043735

Meier, M. F. (1958). The mechanics of crevasse formation. *International Association of Scientific Hydrology Publication*, *46*, 500–508.

Moon, T., Joughin, I., Smith, B., & Howat, I. (2012). 21st-century evolution of Greenland outlet glacier velocities. *Science*, *336*(6081), 576–578. https://doi.org/10.1126/science.1219985

Moon, T., Joughin, I., Smith, B., van den Broeke, M. R., van de Berg, W. J., Noël, B., & Usher, M. (2014). Distinct patterns of seasonal Greenland glacier velocity. *Geophysical Research Letters*, *41*(20), 7209–7216. https://doi.org/10.1002/2014GL061836

Morlighem, M., Williams, C. N., Rignot, E., An, L., Arndt, J. E., Bamber, J. L., Catania, G., Chauché, N., Dowdeswell, J. A., Dorschel, B., Fenty, I., Hogan, K., Howat, I., Hubbard, A., Jakobsson, M., Jordan, T. M., Kjeldsen, K. K., Millan, R., Mayer, L., … Zinglersen, K. B. (2017). BedMachine v3: Complete Bed Topography and Ocean Bathymetry Mapping of Greenland From Multibeam Echo Sounding Combined With Mass Conservation. *Geophysical Research Letters*, 2017GL074954. https://doi.org/10.1002/2017GL074954

Mottram, R. H., & Benn, D. I. (2009). Testing crevasse-depth models: A field study at Breiðamerkurjökull, Iceland. *Journal of Glaciology*, *55*(192), 746–752. https://doi.org/10.3189/002214309789470905

Mouginot, J., & Rignot, E. (2019). *Glacier catchments/basins for the Greenland Ice Sheet* (Version 1, p. 4137543 bytes) [dataset]. Dryad. https://doi.org/10.7280/D1WT11

Müller, L., Horwath, M., Scheinert, M., Mayer, C., Ebermann, B., Floricioiu, D., Krieger, L., Rosenau, R., & Vijay, S. (2021). Surges of Harald Moltke Bræ, north-western Greenland: Seasonal modulation and initiation at the terminus. *The Cryosphere*, *15*(7), 3355–3375. https://doi.org/10.5194/tc-15-3355-2021

Noël, B., van de Berg, W. J., Lhermitte, S., & van den Broeke, M. R. (2019). Rapid ablation zone expansion amplifies north Greenland mass loss. *Science Advances*, *5*(9), eaaw0123. https://doi.org/10.1126/sciadv.aaw0123

Parizek, B. R., Christianson, K., Alley, R. B., Voytenko, D., Vaňková, I., Dixon, T. H., Walker, R. T., & Holland, D. M. (2019). Ice-cliff failure via retrogressive slumping. *Geology*, *47*(5), 449–452. https://doi.org/10.1130/G45880.1

Phillips, T., Rajaram, H., & Steffen, K. (2010). Cryo-hydrologic warming: A potential mechanism for rapid thermal response of ice sheets. *Geophysical Research Letters*, *37*(20). http://onlinelibrary.wiley.com/doi/10.1029/2010GL044397/full

Poinar, K., Joughin, I., Lilien, D., Brucker, L., Kehrl, L., & Nowicki, S. (2017). Drainage of Southeast Greenland Firn Aquifer Water through Crevasses to the Bed. *Frontiers in Earth Science*, *5*. https://doi.org/10.3389/feart.2017.00005

Porter, C., Howat, I., Husby, E., Noh, M.-J., Khuvis, S., Danish, E., Tomko, K., Gardiner, J., Negrete, A., Yadav, B., Klassen, J., Kelleher, C., Cloutier, M., Bakker, J., Enos, J., Arnold, G., Bauer, G., & Morin, P. (2022). *EarthDEM - Strips, Version 1* [dataset]. Harvard Dataverse. https://doi.org/10.7910/DVN/LHE9O7

Porter, C., Howat, I., Noh, M.-J., Husby, E., Khuvis, S., Danish, E., Tomko, K., Gardiner, J., Negrete, A., Yadav, B., Klassen, J., Kelleher, C., Cloutier, M., Bakker, J., Enos, J., Arnold, G., Bauer, G., & Morin, P. (2022). *ArcticDEM - Strips, Version 4.1* [dataset]. Harvard Dataverse. https://doi.org/10.7910/DVN/C98DVS

Reeh, N. (2017). Greenland Ice Shelves and Ice Tongues. In L. Copland & D. Mueller (Eds.), *Arctic Ice Shelves and Ice Islands* (pp. 75–106). Springer Netherlands. https://doi.org/10.1007/978-94-024-1101-0_4

Rouault, E., Warmerdam, F., Schwehr, K., Kiselev, A., Butler, H., Łoskot, M., Szekeres, T., Tourigny, E., Landa, M., Miara, I., Elliston, B., Chaitanya, K., Plesea, L., Morissette, D., Jolma, A., & Dawson, N. (2023). *GDAL* (v3.7.1) [Computer software]. Zenodo. https://doi.org/10.5281/ZENODO.5884351

Shiggins, C. J., Lea, J. M., & Brough, S. (2023). Automated ArcticDEM iceberg detection tool: Insights into area and volume distributions, and their potential application to satellite imagery and modelling of glacier–iceberg–ocean systems. *The Cryosphere*, *17*(1), 15–32. https://doi.org/10.5194/tc-17-15-2023

Slater, D. A., & Straneo, F. (2022). Submarine melting of glaciers in Greenland amplified by atmospheric warming. *Nature Geoscience*, 1–6. https://doi.org/10.1038/s41561-022-01035-9

Sun, S., Cornford, S. L., Moore, J. C., Gladstone, R., & Zhao, L. (2017). Ice shelf fracture parameterization in an ice sheet model. *The Cryosphere*, *11*(6), 2543–2554. https://doi.org/10.5194/tc-11-2543-2017

Thompson, S. S., Cook, S., Kulessa, B., Winberry, J. P., Fraser, A. D., & Galton-Fenzi, B. K. (2020). Comparing satellite and helicopter-based methods for observing crevasses, application in East

Antarctica. *Cold Regions Science and Technology*, *178*, 103128. https://doi.org/10.1016/j.coldregions.2020.103128

Trantow, T., & Herzfeld, U. C. (2018). Crevasses as Indicators of Surge Dynamics in the Bering Bagley Glacier System, Alaska: Numerical Experiments and Comparison to Image Data Analysis. *Journal of Geophysical Research: Earth Surface*, *123*(8), 1615–1637. https://doi.org/10.1029/2017JF004341

van der Veen, C. J. (1998). Fracture mechanics approach to penetration of surface crevasses on glaciers. *Cold Regions Science and Technology*, *27*(1), 31–47. https://doi.org/10.1016/S0165-232X(97)00022-0

van der Veen, C. J. (1999). Crevasses on glaciers. *Polar Geography*, *23*(3), 213–245. https://doi.org/10.1080/10889379909377677

Van Wyk de Vries, M., Lea, J. M., & Ashmore, D. W. (2023). Crevasse density, orientation and temporal variability at Narsap Sermia, Greenland. *Journal of Glaciology*, 1–13. https://doi.org/10.1017/jog.2023.3

Vaughan, D. G. (1993). Relating the occurrence of crevasses to surface strain rates. *Journal of Glaciology*, *39*(132), 255–266. https://doi.org/10.3189/S0022143000015926

Vijay, S., King, M. D., Howat, I. M., Solgaard, A. M., Khan, S. A., & Noël, B. (2021). Greenland ice-sheet wide glacier classification based on two distinct seasonal ice velocity behaviors. *Journal of Glaciology*, 1–8. https://doi.org/10.1017/jog.2021.89

Williams, J. J., Gourmelen, N., & Nienow, P. (2021). Complex multi-decadal ice dynamical change inland of marine-terminating glaciers on the Greenland Ice Sheet. *Journal of Glaciology*, 1–14. https://doi.org/10.1017/jog.2021.31

Young, T. J., Christoffersen, P., Bougamont, M., Tulaczyk, S. M., Hubbard, B., Mankoff, K. D., Nicholls, K. W., & Stewart, C. L. (2022). Rapid basal melting of the Greenland Ice Sheet from surface meltwater drainage. *Proceedings of the National Academy of Sciences*, *119*(10), e2116036119. https://doi.org/10.1073/pnas.2116036119

Extended Data

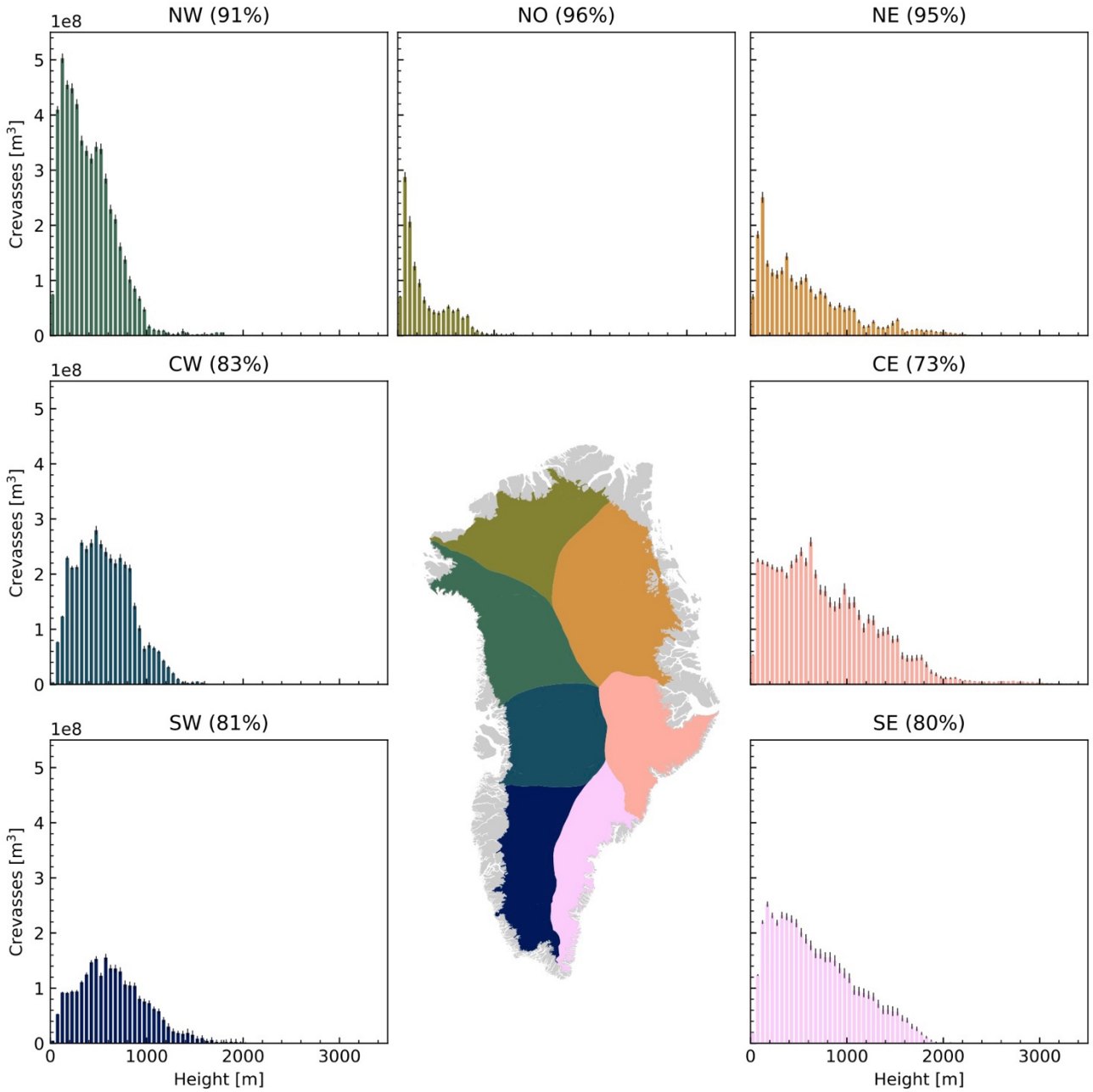

Extended Data Fig. 1: **Histograms of sectoral crevasse volume in 2021 by surface elevation**. Error bars represent 2σ uncertainty. Percentages in figure headings represent proportional data coverage of sector.

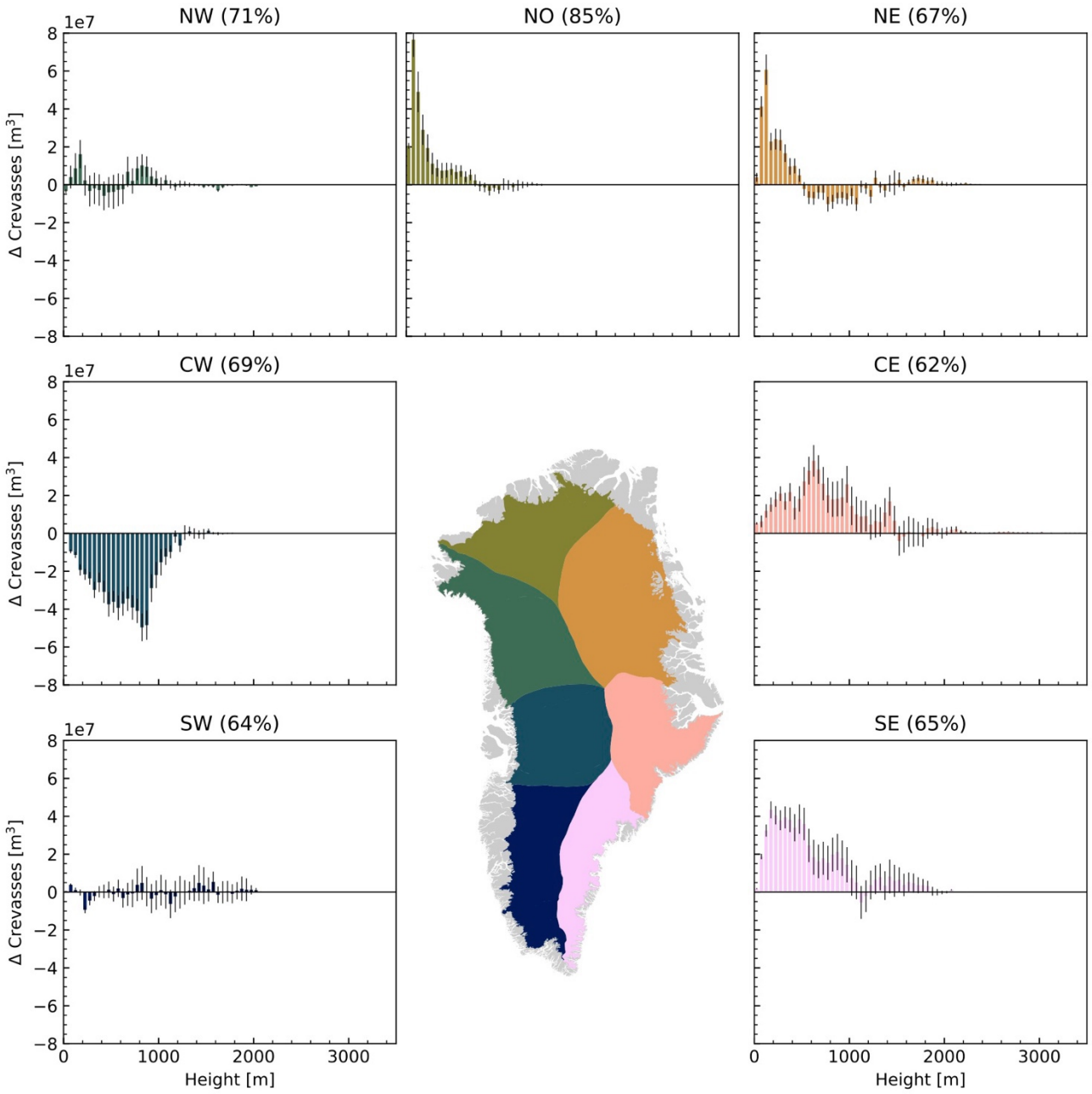

690

Extended Data Fig. 2: **Histograms of sectoral crevasse volume change between 2016-2021 by surface elevation**. Error bars represent 2σ uncertainty. Percentages in figure headings represent proportional data coverage of sector.

695

Extended Data Table 1: Sectoral and total crevasse volumes for 2021. Discharge represents 2017-2021 average.

Total Sector Area

Sector	SW	CW	NW	NO	NE	CE	SE	Total
Total Area (km^2)	83825	46784	48140	50103	82405	32150	54442	397849

2021 Coverage

Sector	SW	CW	NW	NO	NE	CE	SE	Total
Percentage Cover	81%	83%	91%	96%	95%	73%	80%	86%
Volume (m^3)	2.52+E09	4.13+E09	5.42+E09	1.28+E09	2.42+E09	5.55+E09	4.66+E09	25.98+E09
Uncertainty (2σ, m^3)	1.92+E08	1.33+E08	1.76+E08	0.97+E08	1.72+E08	2.81+E08	2.53+E08	1.30+E09

2016 Coverage

Sector	SW	CW	NW	NO	NE	CE	SE	Total
Percentage Cover	81%	81%	76%	86%	67%	69%	68%	75%
Volume (m^3)	2.77+E09	4.54+E09	5.38+E09	1.04+E09	1.82+E09	4.97+E09	3.55+E09	24.06+E09
Uncertainty (2σ, m^3)	2.11+E08	1.32+E08	1.48+E08	0.73+E08	1.14+E08	2.41+E08	2.05+E08	1.12+E09

2016 – 2021 Change

Sector	SW	CW	NW	NO	NE	CE	SE	Total
Percentage Cover	64%	69%	71%	85%	67%	62%	65%	68%

2016 Overlapping Volume (m^3)	2.12+E09	4.43+E09	4.65+E09	1.00+E09	1.79+E09	4.59+E09	3.30+E09	21.89+E09
2016 Uncertainty (2σ, m^3)	1.53+E08	1.24+E08	1.32+E08	0.71+E08	1.10+E08	2.18+E08	1.95+E08	1.00E+09
2021 Overlapping Volume (m^3)	2.13+E09	3.81+E09	4.70+E09	1.26+E09	1.93+E09	5.11+E09	3.90+E09	22.82+E09
2021 Uncertainty (2σ, m^3)	1.61+E08	1.17+E08	1.40+E08	0.90+E08	1.19+E08	2.45+E08	2.09+E08	1.09+E09
Difference Volume (m^3)	0.04+E08	-6.30 +E08	0.39+E08	2.53+E08	1.48+E08	5.19+E08	6.00+E08	9.32+E08
Difference Uncertainty (2σ, m^3)	2.20+E08	1.40+E08	1.58+E08	1.01+E08	1.43+E08	2.81+E08	2.58+E08	13.01+E08
Difference Volume (%)	0.2	-14.2	0.8	25.3	8.3	11.3	18.2	4.3
Difference Uncertainty (%)	10.4	3.2	3.4	10.1	8.0	6.1	7.8	5.9
Significant	N	Y	N	Y	Y	Y	Y	N

710